JOURNAL OF AIRCRAFT
Vol. 41, No. 5, September–October 2004

Engineering Notes

ENGINEERING NOTES are short manuscripts describing new developments or important results of a preliminary nature. These Notes cannot exceed 6 manuscript pages and 3 figures; a page of text may be substituted for a figure and vice versa. After informal review by the editors, they may be published within a few months of the date of receipt. Style requirements are the same as for regular contributions (*see inside back cover*).

Near-Wake Characteristics of an Oscillating NACA 4412 Airfoil

Jo Won Chang*
Hankuk Aviation University,
Kyonggido 412-791, Republic of Korea

I. Introduction

UNSTEADY airflow over oscillating airfoils has been studied by many researchers in recent years.[1,2] The airflow behind a propeller and the wake of a helicopter blade are disturbed by unsteady incoming flows. Previous researchers[3,4] in this area have already revealed that the characteristics of the near wake are highly influenced by reduced frequency, amplitude of oscillation, mean incidence, and airfoil shapes. The trailing vortex wake is related to the prediction of these aerodynamic loads. McCrosky[5] focused on the role of unsteady effects in two-dimensional oscillating airfoils, including dynamic stall vortex formation. He reported that the effects of the Reynolds number on dynamic stall are small at low Mach numbers but the reduced frequency and amplitude are large. Anderson et al.[6] provided force and power data and visualization data to classify the principal characteristics of the flow around and in the wake of a flapping NACA 0012 airfoil. They showed that high efficiency accompanied by significant thrust development is associated with the generation of moderately strong leading-edge vortices, which subsequently amalgamate with trailing-edge vorticity, leading to the formation of a reverse Kármán street.

Both the axial velocity and turbulence properties of the wakes play a significant role in the noise generation and efficiency of the airfoil. Hence, the study of Reynolds-number effects on the near wake of an oscillating airfoil is necessary in the design of efficient airfoils. The sinusoidal oscillation of airfoils that are generating incompressible flows at low Reynolds number has especially been of increasing interest. This interest has been a result of the desire to improve the design of jet-engine fan blades and propellers at high altitudes. The inboard sections of helicopter rotor blades, wind-turbine rotors, and scaled-down model airplanes also represent applications where performance at low Reynolds numbers is important. Many significant aerodynamic problems[7] occur below a chord Reynolds number of about 5.5×10^5. It is important to investigate the flow over the airfoil because the near wake of an oscillating airfoil is closely related to flow phenomena in airfoil surroundings. It is well known that transition and separation over the airfoil are highly sensitive to the Reynolds number. Most studies focus on the behavior of the boundary layer of the stationary airfoil surface, for example, laminar separation, transition, turbulent reattachment, and bubble bursting, due to its significant influence on aerodynamic performance.

The primary objective of the present research is to examine Reynolds-number effects in the near-wake region of an oscillating NACA 4412. Therefore, the present study describes and discusses the instantaneous velocity field and the turbulence intensity in the near-wake region at different Reynolds numbers.

II. Experimental Setup and Procedure

The tests were conducted in a closed-circuit wind tunnel with a square cross section of 0.9×0.9 m and with a test-section length of 2.1 m. The cambered NACA 4412 airfoil was selected for this experiment. The chord length and span of the airfoil model were 0.25 and 0.85 m, respectively. Measurements were made at freestream velocities of 3.4, 12.4, and 26.2 m/s. The corresponding Reynolds numbers based on the chord length were 5.3×10^4, 1.9×10^5, and 4.1×10^5, respectively. Nondimensional reduced frequency K represents the ratio of two time scales: one imposed by the pitching motion, $1/2\pi f$, and the other by the freestream velocity and the airfoil chord, $C/2U_\infty$.

The frequency of oscillation was adjusted to fix a reduced frequency of $K = 0.1$, which many researches[8,9] have done. Therefore, frequencies of oscillation of the airfoil according to freestream velocities were 0.4, 1.6, and 3.2 Hz. Under these test conditions, the freestream turbulent level was about 0.3%. Pitching oscillation about the quarter-chord axis was driven by a variable-speed ac motor and crank-connecting-rod mechanism. The instantaneous angle of attack varied according to $\alpha = \alpha_0 + \alpha_1 \sin 2\pi f t$, where the mean incident angle α_0 and the oscillation amplitude α_1 were set at 0 and 6 deg, respectively. Thus, the instantaneous angle of attack varied from -6 to $+6$ deg.

The coordinate was aligned so that the X coordinate is the main flow direction and the Y coordinate is the normal to the airfoil chord when the angle of attack is zero. The probe was mounted on a support in the center of the airfoil span. The wake profiles were measured at four downstream stations: $X/C = 0.03$, 0.08, 0.15, and 0.5. The probe was traversed in a nondimensional length Y/C ranging from -0.8 to $+0.57$. The measurement positions along the Y axis were taken at 2-mm intervals from the wake center and at intervals from 4 to 10 mm starting outside the wake region.

Dantec's StreamLine System hot-wire anemometer, MetraByte's DAS1601, and a simultaneous sampling and hold unit (SSH-4A) were used for these measurements. The X-type hot-film probe (55R51) was adopted to measure the velocities and their fluctuations. Dantec's calibration unit (Type 90H10) was used for the velocity and directional calibration to obtain sensitivity coefficients of k_i (yaw factor). Typical values of the sensitivity coefficient k_i were 0.28 and 0.32, respectively. One hundred twenty samples of velocity data distributed evenly over one period of oscillation were taken at a given probe position with sampling frequencies of 48, 192, and 384 Hz according to the period of oscillation. The trigger signal for phase averaging was recorded simultaneously with the velocity signals at the instantaneous angle of attack $\alpha = 0$ deg. Test results showed that about 150 ensembles were sufficient to yield converged values of mean velocity and its fluctuations. For each phase angle, 300 ensembles were used for averaging.

The velocity measurement uncertainties in the streamwise velocities were about the 2.0% at 20:1 odds. The uncertainties of the X and Y positioning and instantaneous angle of attack were within

Received 26 October 2003; revision received 1 February 2004; accepted for publication 4 February 2004.

*Assistant Professor, Department of Aeronautical Science and Flight Operation, 200-1, Hwajeon-Dong, Dukyang-Gu, Goyang City; jwchang@hau.ac.kr. Member AIAA.

0.005 mm and ±0.1 deg, respectively. A thermocouple probe monitored temperature variation during the run time of the unsteady test. The temperature variations during the run time were within ±1.5°C. The compensation of hot-film output for the change of fluid temperature was done according to Kanevce and Oka's expression.[10]

III. Results and Discussion

The term "upstroke motion" refers to situations when the nose of the airfoil is moving upward, and the term "downstroke motion" refers to situations when there is a downward movement of the nose. *u* and *d* represent upstroke and downstroke, respectively, when they are coupled with values for the angle of attack. In other words, when the phase angle is within the range 0 deg $< 2\pi f t \leq 90$ deg and 270 deg $< 2\pi f t \leq 360$ deg, the airfoil motion is called "upstroke." When the phase angle is 90 deg $< 2\pi f t \leq 270$ deg, the airfoil motion is said to be a "downstroke" during the change of phase angles from 0 to 360 deg.

Figure 1 illustrates the profiles of the normalized streamwise velocity (u/U_∞) at $\alpha = 0$, +4, and −4 deg. Although the instantaneous angle of attack is the same for both Figs. 1a and 1d, the streamwise velocity profiles are different. This shows that the velocity signals at downstream stations reflect the data that originated at an earlier phase angle of the airfoil oscillation. The term "true instantaneous angles of attack" refers to the angle of attack of the airfoil at the earlier moment when the fluid particle appearing at the probe had passed the $X/C = 0.0$ station. Because of these phase lags, the true instantaneous angles of attack at downstream stations were somewhat smaller or larger than the instantaneous angles of attack during oscillating motion. An accurate estimate of the phase lag is rather difficult to obtain because it involves very elaborate measurements to locally quantify the convection velocity at various stations. However, a rather crude approximation to the convection velocity suffices to explain the phase lag for the present work. Park et al.[2] showed that the convection velocity for cases where $K = 0.2$ was estimated to be about $0.6U_\infty$ when $0.5 < X/C < 1.5$. To compensate for the phase lag, it is assumed that the convection velocity during oscillating motion for cases where $K = 0.1$ is approximately equal to $0.6U_\infty$ when $0.03 < X/C < 0.5$. At $\alpha = 0$ deg, the true instantaneous angles of attack during the oscillation at $X = 0.5C$ are about −1.0 deg *u* and 0.9 deg *d*, respectively.

The streamwise velocity pattern of Fig. 1a is very similar to that of Fig. 1f. The streamwise velocity during the upstroke motion at $\alpha = 0$ deg has almost the same pattern as that during the upstroke motion at a negative angle of attack. This is why the true instantaneous angles of attack, compensated for phase lag during the upstroke

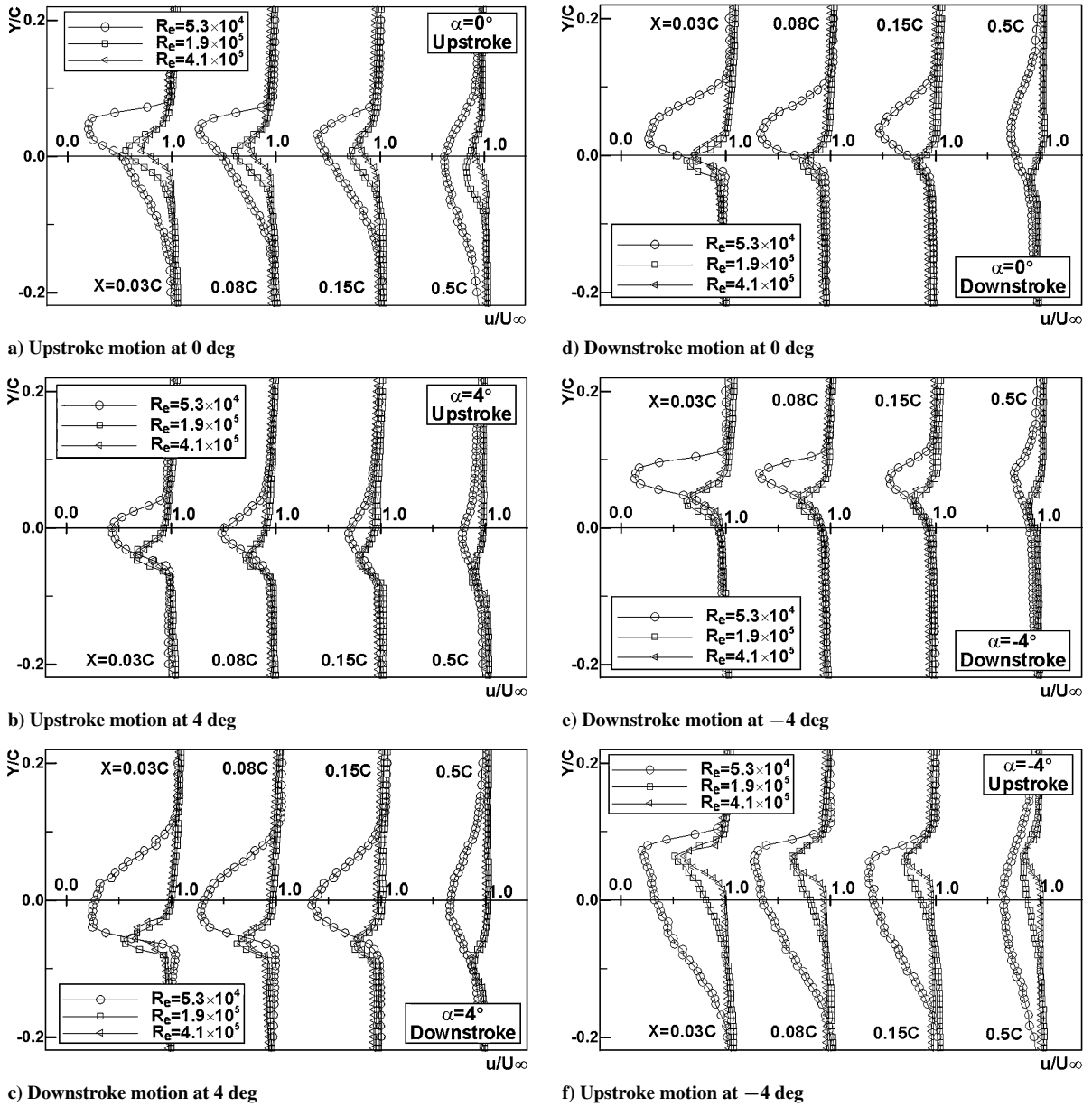

a) Upstroke motion at 0 deg

b) Upstroke motion at 4 deg

c) Downstroke motion at 4 deg

d) Downstroke motion at 0 deg

e) Downstroke motion at −4 deg

f) Upstroke motion at −4 deg

Fig. 1 Streamwise velocity profiles (u/U_∞) at $K = 0.1$.

motion, are negative. Therefore, we can comment that these patterns result from both a camber effect, known as the airfoil-shape effect, and a Reynolds-number effect.

Although the instantaneous angle of attack is the same for both Figs. 1b and 1c, the velocity defects were different. At $\alpha = 4$ deg, the true instantaneous angles of attack during the upstroke and downstroke motion at $X = 0.5C$ are about 3.4 deg u and 4.6 deg d, respectively. This indicates that the true instantaneous angle of attack compensated for by phase lags during the upstroke motion was a little smaller than 4 deg and was a little bigger than 4 deg during the downstroke motion. The wake characteristics clearly demonstrate the hysteretic property between upstroke and downstroke phases. The difference of velocity defect between Figs. 1b and 1c is caused by the upstroke and downstroke motions leading to the flow phenomenon attached to and separated around the airfoil, as in Refs. 8 and 11.

At $Re = 5.3 \times 10^4$, test results show that the magnitude of the velocity defect and width of the velocity defect are much larger than those in the range between $Re = 1.9 \times 10^5$ and 4.1×10^5. Therefore, the flow over the airfoil after the point of separation is highly disturbed and thus becomes very diffuse in the range of $Re = 5.3 \times 10^4$. However, in the range between $Re = 1.9 \times 10^5$ and 4.1×10^5, we can see that the velocity defect is very small and similar to the Reynolds number as shown in Figs. 1b and 1c. Muller and Batill[12] revealed that, at a certain critical value of the Reynolds number, the turbulent mixing and entrainment processes that follow the laminar separation can no longer increase pressure to a value high enough for reattachment to occur or to form a short bubble. If the Reynolds number is increased sufficiently, the transition location at the stationary airfoil will move forward of the point where laminar separation occurred. Therefore, we conjecture that the Reynolds number $Re = 5.3 \times 10^4$ is low enough to maintain laminar flow over the oscillating airfoil when the freestream turbulence intensity is 0.3%. We point out that a large growth in wake thickness at $Re = 5.3 \times 10^4$ causes a larger drag on the oscillating airfoil. Accordingly, the size of the velocity defect is very large because of laminar separation, resulting in a thicker wake and causing a larger pressure drag. The size of the velocity defect at $Re = 1.9 \times 10^5$ and 4.1×10^5 is very small compared to that at $Re = 5.3 \times 10^4$, resulting in a thinner wake, which subsequently causes less pressure drag. Ohmi et al.[9] investigated the airflow passing an oscillating airfoil by visualization experiments at incidences from 0 to 45 deg, and the Reynolds number based on the chord length was between 1.5×10^3 and 1.0×10^4. Test results showed that the dominant parameter of the flow was the

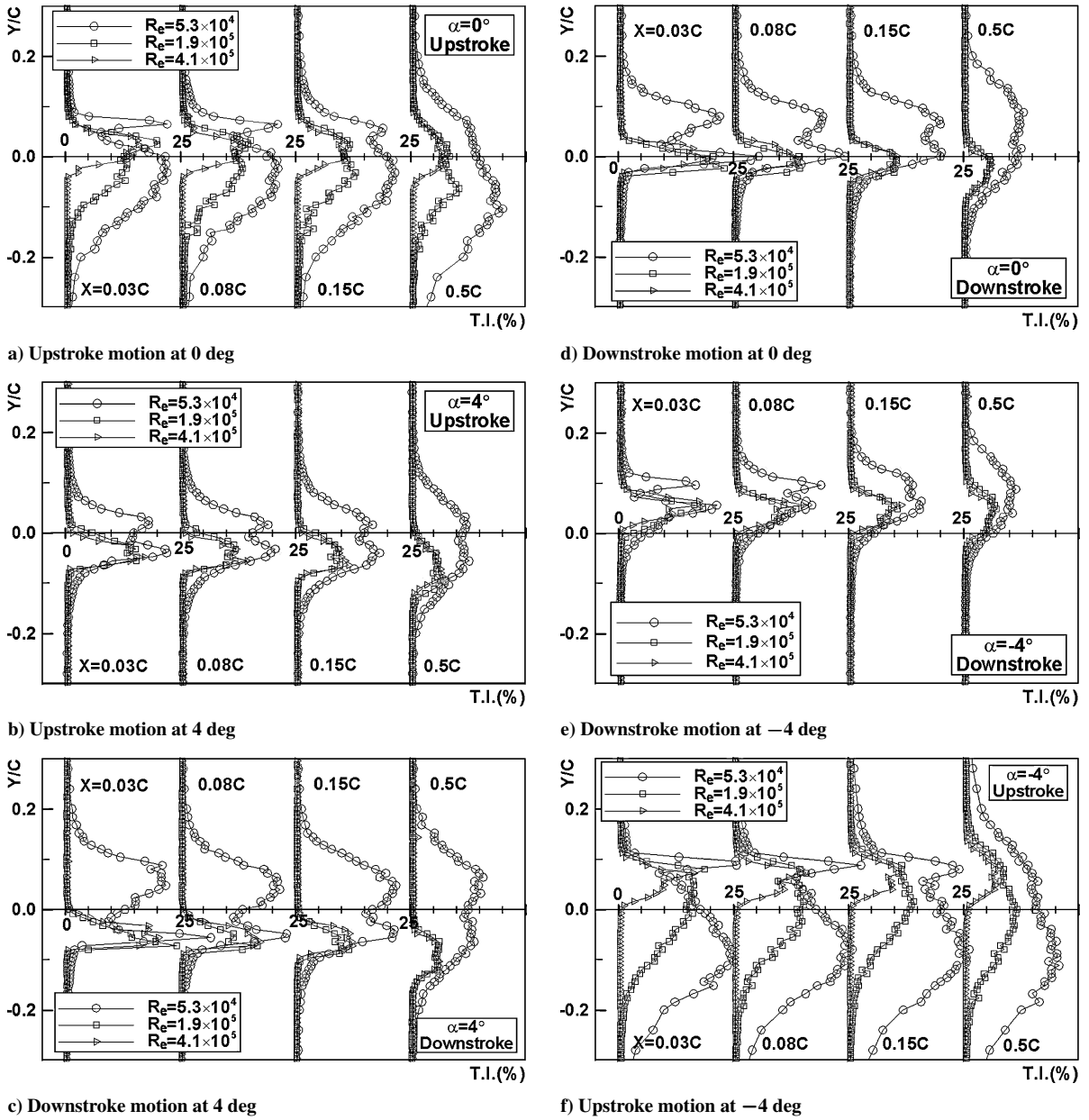

a) Upstroke motion at 0 deg

d) Downstroke motion at 0 deg

b) Upstroke motion at 4 deg

e) Downstroke motion at −4 deg

c) Downstroke motion at 4 deg

f) Upstroke motion at −4 deg

Fig. 2 Turbulence intensity profiles at $K = 0.1$.

reduced frequency in all the incidence ranges, and the effect of the Reynolds number was much less important than that of the other parameters. However, their experiments did not increase to sufficiently large Reynolds numbers. Indeed, the effect of the Reynolds number close to the critical value is apparent: an increasing Reynolds number corresponds to a decreasing axial velocity defect.

The streamwise velocity pattern of Fig. 1d is also very similar to that of Fig. 1c. The streamwise velocity during the downstroke motion at $\alpha = 0$ deg has almost the same pattern as that during the downstroke motion at a positive angle of attack. This is due to the phase lag, which was achieved by a procedure similar to that used in Fig. 1a.

In this study, primary emphasis was placed on the Reynolds-number effects on the near wake of the NACA 4412 airfoil at different Reynolds numbers. We also see that the velocity defect of the downstroke motion at the instantaneous angle of attack of -4 deg (Fig. 1e) is very large at the lowest Reynolds number, 5.3×10^4, but the velocity defect of the same motion did not vary in the range between $Re = 1.9 \times 10^5$ and 4.1×10^5.

In Fig. 1f, the Reynolds-number effect and camber effect, known as the airfoil shape effect, of the NACA 4412 airfoil were remarkable. In the case of upstroke motion at a negative angle of attack, the velocity defect in the lower wake region was considerably different from those in Figs. 1b–1e. The velocity defect in the lower wake region is large because of the separation near the nose in the lower surface. These results may be caused by the slightly sharper-edged nose shape of the lower surface of the NACA 4412 airfoil compared to the nose shape of the upper surface, which moves a separation point toward the nose. More discussions of the camber effect on the near wake of an oscillating airfoil can be found in Ref. 4.

Typical profiles of axial turbulence intensity at $\alpha = 0, +4$, and -4 deg at different Reynolds numbers are depicted in Fig. 2. The turbulence intensity profiles in Fig. 2a with an upstroke motion at $\alpha = 0$ deg, corresponding to the streamwise velocity profile in Fig. 1, were also similar to those in Fig. 2f, which had upstroke motions at negative angles of attack. This means that the hot-film signals at downstream stations reflect the origin of the data at an earlier phase angle of the airfoil oscillation, as in the case of the streamwise velocity profiles in Fig. 1.

In Fig. 2b, the lowest Reynolds number, $Re = 5.3 \times 10^4$, had the largest size and width of turbulence intensity, but there was little difference between $Re = 1.9 \times 10^5$ and 4.1×10^5. The effect of the Reynolds number at $Re = 5.3 \times 10^4$ was quite clear. As alluded to earlier, this may be related to the laminar separation on the airfoil surface at $Re = 5.3 \times 10^4$. Thus, there exists a critical value of the Reynolds number, within the range between $Re = 5.3 \times 10^4$ and 1.9×10^5, which determines the state of the boundary layer before separation.

Test results showed that the oscillating airfoil during the downstroke motion at a positive angle of attack (Fig. 2c) had turbulence intensity relatively broader than that of the upstroke motion (Fig. 2b). The turbulence-intensity profiles in Fig. 2d with a downstroke motion at $\alpha = 0$ deg were also similar to those in Fig. 2c, which had downstroke motions at positive angles of attack. The turbulence intensity with downstroke motion at $\alpha = 0$ deg was very large when $Re = 5.3 \times 10^4$, but the turbulence intensity for the same motion was small and nothing was different between $Re = 1.9 \times 10^5$ and 4.1×10^5. According to the Reynolds number, we believe, the boundary layer will be either laminar or turbulent before separation, which creates different flow phenomena and also produces a critical value of the Reynolds number. The near-wake characteristics of an NACA 4412 airfoil at $\alpha = 0$ deg are different according to the motion direction because of the asymmetric shape of the airfoil, which creates a different separation point at each airfoil surface and phase lag in the near-wake region of the airfoil oscillation.

The degree of flow separation and disturbance at $Re = 5.3 \times 10^4$ was much greater than that in the range between $Re = 1.9 \times 10^5$ and 4.1×10^5. The motion between Figs. 2b and 2e was symmetric about the X axis, but the distributions of turbulence-intensity profiles were not symmetric about the X axis because of the asymmetric shape of the NACA 4412 airfoil.

It indicates that the turbulence-intensity profile in the upstroke motion at $\alpha = -4$ deg was remarkably different from those in Figs. 2b–2e and also shows that the wake in this particular case has undergone quite a different flow history compared to Figs. 2b–2e. In addition, it is important to point out that the size of axial turbulence intensity decreases with the Reynolds number in the near-wake region, as illustrated in Fig. 2f.

Therefore, the near-wake characteristics of an oscillating NACA 4412 airfoil were coupled with both the camber effect associated with up/down stroke motions and the Reynolds-number effect associated with the growth and separation of the boundary layer. This signifies that the flow over the airfoil is highly disturbed, so that the flow becomes very diffuse during upstroke motion at a negative angle of attack.

IV. Conclusions

This experimental study was carried out to measure phase-averaged mean velocity and its turbulent intensity in the near-wake region of an oscillating NACA 4412 airfoil at the Reynolds numbers $Re = 5.3 \times 10^4$, 1.9×10^5, and 4.1×10^5. All cases in these measurements show that the velocity defects were coupled with both the camber effect and the Reynolds-number effect and that the Reynolds-number effect may be associated with the laminar or turbulent boundary layer on the airfoil surface. The near-wake characteristics of an oscillating NACA 4412 airfoil are insensitive to Reynolds numbers between $Re = 1.9 \times 10^5$ and 4.1×10^5. At $Re = 5.3 \times 10^4$, test results show that the magnitude and width of the velocity defect are much larger than those in the range between $Re = 1.9 \times 10^5$ and 4.1×10^5. A critical value of the Reynolds number in the near wake of an oscillating NACA 4412 airfoil, which includes either cases of lamina separation or cases of no separation or turbulent separation, exists in the range between 5.3×10^4 and 1.9×10^5. The near-wake characteristics of the NACA 4412 airfoil at $\alpha = 0$ deg are considerably different depending on motion direction due to the slightly sharper-edged nose shape of the lower surface of the NACA 4412 airfoil compared to the nose shape of the upper surface as well as the phase lag in the near-wake region of the airfoil oscillation.

Acknowledgment

This work was supported by Grant R01-2002-000-00442-0 from the Basic Research Program of the Korea Science and Engineering Foundation.

References

[1]Tatineni, M., and Zhong, X., "Numerical Simulation of Unsteady Low-Reynolds-Number Separated Flows over Airfoils," *AIAA Journal*, Vol. 38, No. 7, 2000, pp. 1295–1300.

[2]Park, S. O., Kim, J. S., and Lee, B. I., "Hot-Wire Measurements of Near Wakes Behind an Oscillating Airfoil," *AIAA Journal*, Vol. 28, No. 1, 1990, pp. 22–28.

[3]Hah, C., and Lakshminaryana, B., "Measurement and Prediction of Mean Velocity and Turbulence Structure in the Near Wake of an Airfoil," *Journal of Fluid Mechanics*, Vol. 115, 1982, pp. 251–282.

[4]Chang, J. W., and Yoon, Y. H., "Camber Effects on the Near Wake of Oscillating Airfoils," *Journal of Aircraft*, Vol. 39, No. 4, 2002, pp. 713–716.

[5]McCrosky, W. J., "Unsteady Airfoils," *Annual Review of Fluid Mechanics*, Vol. 14, 1982, pp. 285–311.

[6]Anderson, J. M., Streitlien, K., Barrett, D. S., and Triantafyllou, M. S., "Oscillating Foils of High Propulsive Efficiency," *Journal of Fluid Mechanics*, Vol. 360, 1998, pp. 41–72.

[7]Mueller, T. J., and Jansen, B. J., Jr., "Aerodynamic Measurements at Low Reynolds Numbers," AIAA Paper 82-0598, March 1982.

[8]Chang, J. W., and Park, S. O., "A Visualization Study of Tip Vortex Roll-Up of an Oscillating Wing," *Journal of Flow Visualization and Image Processing*, Vol. 6, No. 1, 1999, pp. 79–87.

[9]Ohmi, K., Coutanceau, M., Loc, T. P., and Dulieu, A., "Vortex Formation Around an Oscillating and Translating Airfoil at Large Incidence," *Journal of Fluid Mechanics*, Vol. 211, 1990, pp. 37–60.

[10]Kanevce, G., and Oka, S., "Correcting Hot-Wire Reading for Influence of Fluid Temperature Variations," *DISA Information*, No. 15, Oct. 1973, pp. 21–24.

[11]Chang, J. W., and Park, S. O., "Measurements in the Tip Vortex Roll-Up Region of an Oscillating Wing," *AIAA Journal*, Vol. 38, No. 6, 2000, pp. 1092–1095.

[12]Muller, T. J., and Batill, S. M., "Experimental Studies of Separation on a Two-Dimensional Airfoil at Low Reynolds Number," *AIAA Journal*, Vol. 20, No. 4, 1982, pp. 457–463.

Visualized Vortices on Unmanned Combat Air Vehicle Planform: Effect of Reynolds Number

M. Elkhoury* and D. Rockwell†
Lehigh University, Bethlehem, Pennsylvania 18015

I. Introduction

FLOW past an aerodynamic planform at angle of attack generates complex flow patterns due to abrupt changes in sweep angle and to the existence of a wing root. Such planforms generate more than one vortex system. For example, one type of vortex arises from the main fuselage or strake, and another emanates at the wing root. Generally speaking, these vortices can interact with one another. Previous investigations have clearly demonstrated that the development and potential interaction of vortices is a function of Reynolds number. Hebbar et al.[1] characterize the Reynolds number dependence of the vortices on a double delta wing planform. They employ dye visualization, along with laser Doppler velocimetry, to determine details of the flow patterns. Their dye visualization showed a strong dependence on Reynolds number of the onset of vortex breakdown, as well as the interaction of the vortices. At a lower value of Reynolds number, the vortices from the apex of the wing and the wing root interacted with each other, whereas at a higher value, they developed nearly parallel to one another, and their axes did not intersect. Furthermore, the angle of inclination of the wing root vortex changed substantially with Reynolds number. Verhaagen[2] provides an overview of investigations that show similar features of the vortex development and interaction as a function of Reynolds number. His overview also includes oil-film visualization for determination of the corresponding patterns of surface shear stress lines as a function of Reynolds number. Further investigations on the effects of Reynolds number have focused on relatively high values extending from 0.5 to 2.5×10^6, as described by Visser and Washburn[3] and Verhaagen et al.[4] These investigations also included variations of angle of attack. Visser and Washburn[3] focused on the boundary-layer transition on delta wings having a flat surface on the leeward side. The occurrence of transition involved outward movement of the secondary separation line. Furthermore, it was found that the occurrence of transition was strongly correlated with the strength of the vortex, as represented by its circulation evaluated in the crossflow plane. Verhaagen et al.[4] characterized the effect of Reynolds number on the surface pressure coefficient along the leeward surface of the wing and, furthermore, showed the effect of Reynolds number on qualitative visualization, as well as on topological representations of the surface flow patterns.

Unmanned combat air vehicle (UCAV) planforms typically involve relatively low values of sweep angle of both the fuselage (main body) and the wing extension. Little attention has been devoted to understanding the flow structure on simple delta wings of low sweep angle, let alone more complex configurations such as UCAV planforms. The general issue, therefore, arises as to the dependence of the flow patterns on a UCAV on both the Reynolds number and the angle of attack. The aim of the present investigation is to provide various measures of the visualized dye patterns, including the degree of interaction of vortices, the onset of vortex breakdown, and the effective sweep angle of the wing root vortex, as a function of both Reynolds number and angle of attack.

II. Experimental System and Techniques

Experiments were performed in a large-scale water channel, with a test section 927 mm wide, 610 mm deep, and 4928 mm long. The flow velocity was varied over the range of 27–214 mm/s. The chord of the planform was $C = 188$ mm, and, therefore, values of Reynolds number Re based on chord ranged from $Re = 5 \times 10^3$ to 4×10^4.

The planform approximated the Boeing X-45 UCAV. An outline of this planform is given in Fig. 1. The wing had a thickness of 3.2 mm and was beveled on its windward side at an angle of 30 deg. The wing was held in position by a streamlined strut of thickness 2.5 mm. Extensive visualization in conjunction with particle image velocimetry ascertained that the position of this strut did not have an effect on the flow patterns on the leeward surface of the wing. Dye ports were located near the tip of the apex of the wing, that is, at a distance of 2.0 mm from the tip, with the openings on the leeward surface.

Similarly, ports were located at the wing root. By allowing dye to flow simultaneously from these four ports, it was possible to examine simultaneously the overall symmetry of the patterns, as well as the degree of interaction of the vortex systems. The wing was mounted at negative angle of attack, with the bevel on the windward surface, such that images of the dye could be recorded by a camera oriented such that its viewing axis extended upward through the bottom surface of the water channel. This high-resolution charge-coupled device (CCD) camera had an array of 1024×1024 pixels, of which 1008×1016 were light sensitive. Images were recorded at a rate of 30 frames per second. Representative excerpts from the visualization sequences are shown herein.

III. Overview of Visualized Patterns

Figures 2a and 2b show patterns of dye visualization, over a Reynolds number range of $Re = 5 \times 10^3$–4×10^4, for angles of attack $\alpha = 4$, 7, 10, and 13 deg. Consider the vortices formed from the fuselage (main body) of the planform. It is evident that the onset of either a pronounced undulation of the dye marker or an abrupt

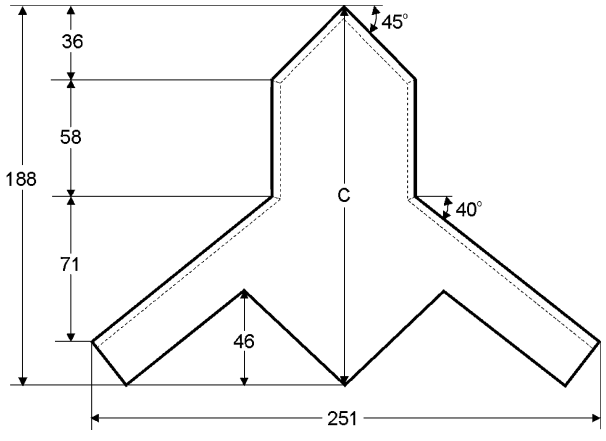

Fig. 1 Model geometry (dimensions in millimeters).

Received 5 November 2003; revision received 9 March 2004; accepted for publication 10 March 2004.

*Research Assistant, Department of Mechanical Engineering and Mechanics, 356 Packard Laboratory, 19 Memorial Drive West. Student Member AIAA.

†Paul B. Reinhold Professor, Department of Mechanical Engineering and Mechanics, 356 Packard Laboratory, 19 Memorial Drive West; dor0@lehigh.edu.